The Astrophysical Journal, 671:842–852, 2007 December 10

EMISSION LINE VARIABILITY OF THE ACCRETING YOUNG BROWN DWARF 2MASSW J1207334−393254: FROM HOURS TO YEARS

Beate Stelzer
INAF-Osservatorio Astronomico di Palermo, Piazza del Parlamento 1, 90134 Palermo, Italy; stelzer@astropa.unipa.it

Alexander Scholz
SUPA, School of Physics and Astronomy, University of Saint Andrews, North Haugh, Saint Andrews, Fife KY 16 9SS, UK

and

Ray Jayawardhana
Department of Astronomy and Astrophysics, University of Toronto, 50 Saint George Street, Toronto, ON M5S 3H4, Canada
Received 2007 April 29; accepted 2007 July 5

ABSTRACT

We have obtained a series of high-resolution optical spectra for 2MASSW J1207334−393254 (2M 1207). Two consecutive observing nights at the ESO Very Large Telescope with the Ultraviolet and Visual Echelle Spectrograph yielded a time series with a resolution of ∼12 minutes. Additional high-resolution optical spectra were obtained months apart at the Magellan Clay telescope using the Magellan Inamori Kyocera Echelle (MIKE) instrument. Combined with previously published results, these data allow us to investigate changes in the emission line spectrum of 2M 1207 on timescales of hours to years. Most of the emission line profiles of 2M 1207 are broad, in particular that of Hα, indicating that the dominant fraction of the emission must be attributed to disk accretion rather than to magnetic activity. From the Hα 10% width, we deduce a relatively stable accretion rate between $10^{-10.1}$ and $10^{-9.8}\,M_{\odot}\,\mathrm{yr}^{-1}$ for two nights of consecutive observations. Therefore, either the accretion stream is nearly homogeneous over (sub)stellar longitude, or the system is seen face-on. Small but significant variations are evident throughout our near-continuous observation, and they reach a maximum after ∼8 hr, roughly the timescale on which maximum variability is expected across the rotation cycle. Together with past measurements, we confirm that the accretion rate of 2M 1207 varies by more than 1 order of magnitude on timescales of months to years. Such variable mass accretion yields a plausible explanation for the observed spread in the $\dot{M}$-M diagram. The magnetic field required to drive the funnel flow is on the order of a few hundred G. Despite the obvious presence of a magnetic field, neither radio nor X-ray emission has been reported for 2M 1207. It is possible that strong accretion suppresses magnetic activity in brown dwarfs, similar to the findings for higher mass T Tauri stars.

Subject headings: accretion, accretion disks — circumstellar matter — line: formation — line: profiles — planetary systems — stars: low-mass, brown dwarfs

1. INTRODUCTION

In recent years, there is increasing evidence that young brown dwarfs evolve similarly to their higher mass counterparts, the T Tauri stars (TTSs). In particular, their formation process includes a phase of mass accretion from a circumstellar disk, whose presence is probed by infrared emission in excess of the photosphere (e.g., Natta et al. 2002; Jayawardhana et al. 2003a; Luhman et al. 2005; Allers et al. 2006). Spectroscopic features, such as the strength and shape of Hα emission, directly trace the accreting material. In the stellar regime, "weak TTSs"' have no optically thick circumstellar matter, and their Hα emission is purely chromospheric. In "classical TTSs," the line emission is dominated by contributions from accretion. In addition to displaying much stronger lines, their line profiles are broader due to the high velocities in the accreting gas and due to Stark broadening (Muzerolle et al. 2001). Winds may play a role as well, and are recognized by blueshifted absorption components and forbidden emission lines (Mundt 1984; Edwards et al. 1987; Hamann 1994; Hartigan et al. 1995). Analogous observations have been made for brown dwarfs, where classical TTS-like Hα emission persists down to the deuterium burning limit (Mohanty et al. 2005). Forbidden emission lines, which trace outflows, have been reported from a small number of brown dwarfs (e.g., Fernández & Comerón 2001; Barrado y Navascués et al. 2004).

Brown dwarfs are intrinsically faint objects, and therefore a detailed study of magnetic activity and accretion in young brown dwarfs is restricted to the most nearby ones. A particularly well-suited playground is the TW Hya association (TWA), with four confirmed brown dwarfs at an age of ∼8 Myr and a distance of ∼50 pc. 2MASSW J1207334−393254 (hereafter 2M 1207) is the best-studied among the brown dwarfs in the TWA. Its youth was confirmed by low gravity and lithium absorption, and its TWA membership by radial velocity and proper motion studies (Gizis 2002; Mohanty et al. 2003; Scholz et al. 2005b). Mamajek (2005) has revised the previous distance estimate of 2M 1207 using the moving cluster method, resulting in 53 ± 6 pc. 2M 1207 is the oldest brown dwarf known to actively accrete from a disk, and thus represents a benchmark in constraining the disk lifetimes in the substellar regime. The object has recently aroused strong interest because of the discovery of a planetary mass companion (Chauvin et al. 2004, 2005). This companion is at a separation of 40 AU and is not expected to influence the magnetic and accretion activity of the brown dwarf.

Stellar astronomers are intrigued by 2M 1207, as it is the closest known brown dwarf with a disk. No substantial L' excess was detected by Jayawardhana et al. (2003a), but mid-IR photometry did establish the presence of circumstellar material (Sterzik et al. 2004). This is also corroborated by *Spitzer* photometry, where 2M 1207 is detected in all IRAC bands and at 24 μm above

photospheric levels (Riaz et al. 2006). The spectral energy distribution of 2M 1207 shows evidence for dust evolution, similar to the higher mass disk-bearing TTSs in the TWA. 2M 1207 is therefore a lower mass analog of the classical TTS.

Strong Hα emission was reported just as 2M 1207 was identified as a TWA candidate (Gizis 2002). Subsequent high-resolution spectra have shown that the Hα profile is broadened and asymmetric, and thus displays characteristic signatures of accretion (Mohanty et al. 2003). The Hα equivalent width measured by Mohanty et al. (2003) was only about one-tenth of the earlier value obtained by Gizis (2002), and this variability was interpreted as a sign of a variable mass accretion rate. In a subsequent study of emission line variability aimed at constraining these variations, 2M 1207 presented dramatic changes in the shape and intensity of its Hα line in data obtained two months apart (Scholz et al. 2005a). The observed profile variability was consistent with a scenario of asymmetric accretion with a direct view into the (magnetic) funnel flow (Scholz & Jayawardhana 2006). In this picture, variability is also expected on the timescale of the rotation period ($\sim$1 day), as the hot accretion spots are corotating with the star. Existing data have remained inconclusive in this respect due to poor sampling. Therefore, we have collected new high spectral resolution data with the aim of monitoring the Hα variability on shorter timescales.

Here we present the results obtained during two consecutive nights of observation, and from five additional spectra taken weeks to months apart. The observations are described in § 2. In § 3, we present a detailed analysis of the characteristics of the Hα emission and other prominent emission lines in the optical spectrum of 2M 1207. The results are discussed in § 4, where the spectral variability is examined on various timescales from hours to years. Estimates for the accretion rate and the magnetic field strength of 2M 1207 are presented and put in context with other (sub)stellar objects. Finally, we compare the accretion and activity characteristics of all known brown dwarfs in the TWA. Concluding remarks are found in § 5.

2. OBSERVATIONS

2M 1207 was observed during two nights, 2006 May 8 and 9, with the Ultraviolet and Visual Echelle Spectrograph (UVES) at the ESO VLT 2 in the dichroic mode that covers the full spectral range of UVES by simultaneous use of both the blue and the red arm. We used the standard setting, with DICHR#2 centered at 437 nm for the blue arm and at 760 nm for the red arm. This setup yielded simultaneous spectral coverage from 3730–4990 Å on the blue chip and from 5650–9460 Å on the red mosaic. A slit width of 0.8″ was chosen, resulting in a resolving power $R \approx 50{,}000$. The CCDs were rebinned to 2×2 pixels.

The integration time was 600 s. During the two observing nights, we obtained a total of 59 exposures of 2M 1207 at blue and red wavelengths. Except for some constraints due to calibrations and weather, the frames were taken consecutively, such that the time resolution for the investigation of spectral changes is $\sim$12 minutes over a large part of the observations.

The data were processed with the UVES pipeline implemented in the MIDAS environment (Ballester et al. 2000). Reduction steps included bias subtraction, flat-field correction, and wavelength calibration. The final one-dimensional spectra were corrected for contaminating sky light, and cosmic rays have been removed. Each spectrum was corrected for the radial velocity of 2M 1207 (11.2 km s^{-1}; Mohanty et al. 2003) and for the barycenter motion of the Earth.

We extracted a spectrum from each of the individual science frames. In addition, to increase the signal-to-noise ratio (S/N) for the detection and measurements of weak spectral features, we built averages of each set of four consecutive frames. Thus, the effective exposure times of these merged spectra are 40 minutes. Three individual frames with poor S/N were not considered in the merging process, such that we obtained 14 average spectra from the two nights. The spectra were rebinned to $R = 50{,}000$ around individual emission lines before the scientific analysis was carried out.

In 2006 February and April, we obtained five additional exposures of 2M 1207 using the Magellan Inamori Kyocera Echelle (MIKE) spectrograph at the Magellan Clay telescope on Las Campanas, Chile. These data were reduced using standard routines within IRAF, including bias subtraction, flat-fielding, wavelength and relative flux calibration, and removal of cosmic rays. For more details of the reduction procedure, see Scholz & Jayawardhana (2006). Exposure times for the MIKE spectra were typically 10 minutes, and the nominal resolution is $R \approx 25{,}000$.

3. EMISSION LINE SPECTRUM

3.1. Hα *Emission*

The main aim of this study is to examine the variability of the Hα emission of 2M 1207 with good time resolution and on timescales of $\sim$1 day, which corresponds to its suspected rotation period. An estimate for the period is given by Scholz et al. (2005a). In brief, the rotational velocity of 2M 1207 is $v \sin i = 13 \pm 2$ km s^{-1} (Mohanty et al. 2003). Together with a radius of 0.27 $R_\odot$ extracted from evolutionary models (Chabrier et al. 2000), the period is expected to be $P/\sin i \approx 25.2$ hr. Assuming a random position for the inclination, the most probable value for $\sin i$ is 0.81, and for this value the rotation period is 20.4 hr. Magnetospheric accretion models (Hartmann et al. 1994) have shown that the presence of a red absorption feature in the Balmer lines (frequently seen in 2M 1207; see below) indicates high inclination. For $i \geq 60^\circ$ the expected period is $\geq$22 hr.

The Hα emission of 2M 1207 is thought to be dominated by accretion; the broad wings with velocities of up to $\pm$200 km s^{-1} cannot be explained by magnetic activity, the rotational velocity is comparatively small and cannot be responsible for the broad wings, and signatures for winds are very weak (Mohanty et al. 2005; Whelan et al. 2007).

The most widely used indicator for identifying accreting stars is the equivalent width $W_{\rm eq}$ of the Hα line, where weak emission is due to chromospheric magnetic activity, and strong emission, above a certain threshold of $W_{\rm eq}$, is attributed to accretion. However, its dependence on the continuum level precludes $W_{\rm eq}$ as a universal measure. To take account of the declining continuum for later spectral types, the threshold for $W_{\rm eq}$ that separates accretors from nonaccretors among TTSs is usually adapted in discrete steps from $\sim$5 Å for spectral types earlier than M0 to something like 20 Å for late M-type stars (Martín 1998). Furthermore, equivalent width measurements of faint continuum sources such as brown dwarfs are intrinsically associated with considerable uncertainties. This is due to the low S/N and the presence of overlapping absorption features that form a "pseudocontinuum" that depends on the spectral resolution. To avoid these problems, following a suggestion by White & Basri (2003), the full width at 10% of the peak height ($W_{10\%}$) of Hα has been established as a more reliable accretion indicator; objects with $W_{10\%} > 200$ Å can be considered accretors (Jayawardhana et al. 2003b).

3.1.1. *Profiles and Line Widths*

We use $W_{10\%}$ as the primary accretion indicator, but also examine other parameters that characterize the line intensity and shape. Figure 1 shows the time series of these parameters obtained during

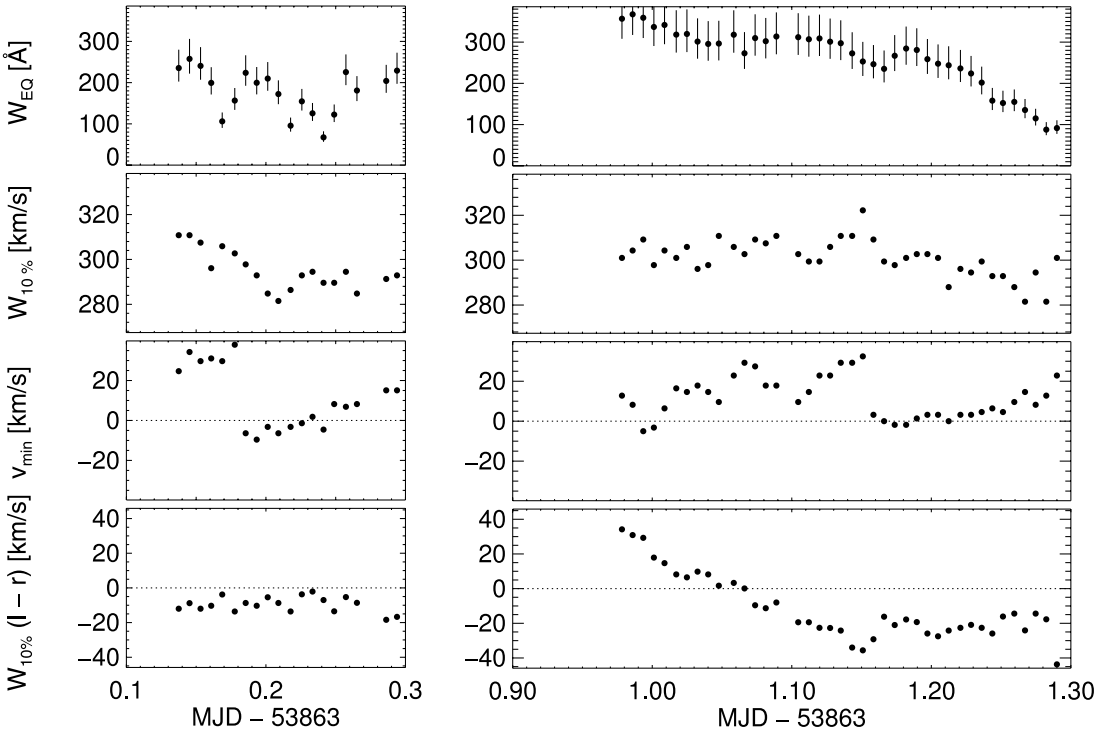

FIG. 1.—Temporal evolution of parameters characterizing the Hα emission of 2M 1207 during 2006 May 8 and 9.

our run with UVES on 2006 May 8 and 9. The 10% width is clearly above the accretion threshold throughout our observation ($W_{10\%} \approx 280$–320 km s^{-1}); on average, it is higher during the second night, in the course of which it slightly declines. The equivalent width has ups and downs during the first night, and has its maximum at the beginning of the second night, after which it declines dramatically and in a continuous way until the end of the observation. The errors in $W_{\rm eq}$ are dominated by the (faint) continuum level. We estimated the uncertainty of the continuum flux by varying the sky extraction area, and found that it is of the order of 15%. Then we computed error bars for $W_{\rm eq}$, assuming for the continuum flux $0.85I_{\rm cont}$ and $1.15I_{\rm cont}$, respectively. Figure 1 shows that when taking into account these uncertainties, the observed variations of $W_{\rm eq}$ remain significant.

The Hα emission is double-peaked throughout all our observations from 2006 February to May. Figure 2 displays the time series of all 14 normalized average line profiles $\langle I_n(\lambda)\rangle$ from the UVES run (2006 May), and Figure 3 shows the 5 normalized profiles obtained with MIKE (2006 February and April). For clarity, in Figures 2 and 3, the individual spectra have been shifted with respect to each other in the vertical direction.

Scholz et al. (2005a) have shown that the double-peaked Hα profile of 2M 1207 can be interpreted as a broad emission line onto which a redshifted absorption component is superposed. For the minimum of the absorption feature, we measure a position that varies in the range $\Delta v_{\rm min} \approx -10$ to $+70$ km s^{-1} with respect to the expected wavelength ($\Delta v_{\rm min} \approx +30$ to $+70$ km s^{-1} in 2006 February, $\Delta v_{\rm min} \approx +10$ km s^{-1} in 2006 April, and $\Delta v_{\rm min} \approx -10$ to $+40$ km s^{-1} in 2006 May). From Figure 1, it appears that twice during the extensive monitoring in 2006 May, $v_{\rm min}$ underwent a discrete jump from high redshift toward the expected line center. These times correspond to line profiles in which the absorption trough is wide and asymmetric, such that the position of the minimum cannot be determined precisely (Fig. 2). As a measure of the asymmetry of the emission component, Figure 1 shows the difference between the 10% width on the blue (*left*) and on the red (*right*) side of $\Delta v = 0$. In the course of the UVES observations, $W_{10\%}(l-r)$ varied from -40 to +40 km s^{-1}. In particular, during the second night the line moved systematically from the blue to the red. This is in contrast to the absorption feature shown above to be redward of $\Delta v = 0$ throughout the observation (cf. also Fig. 2).

We examined the shape of the Hα line and its change in time by modeling each of the 14 average profiles with two quasi-Gaussians, one with positive normalization representing the emission component and one with negative normalization for the absorption component. Each of these has three free parameters (position, width, and normalization). The equivalent widths of the emission $W_{\rm eq;em}$ and the absorption $W_{\rm eq;abs}$ components derived from the fits turn out to be strongly correlated (Fig. 4). Since $W_{\rm eq;em}$ is by definition normalized to the continuum, this relation is not trivial. In Figure 4, we also plot the *observed* flux, i.e., the difference between the flux in the emission profile and the absorption profile, versus the 10% width.

The Hα 10% width of 2M 1207 has been measured at eight epochs so far (see Table 1). In most of the high-resolution spectra collected, 2M 1207 showed $W_{10\%}$ to be clearly above the accretion threshold, although on some occasions there were only marginal signs of accretion ($W_{10\%} \sim 200$ km s^{-1}).

3.1.2. *Quantifying Variability*

To quantify the Hα variability as a function of wavelength, we examined the normalized variance profile

$$\sigma_n^2(\lambda) = \sigma^2(\lambda)/\langle I_n(\lambda)\rangle, \quad (1)$$

where the variance profile $\sigma^2(\lambda) = [1/(N-1)]\sum_{i=1}^{N}[I_{n,i}(\lambda) - \langle I_n(\lambda)\rangle]^2$ measures flux variations across the line profile (Johns & Basri 1995). In the bottom panels of Figure 2, we plot $(\sigma_n^2)^{1/2}$ for three distinct parts of the observation in 2006 May. From left to right are the variances obtained from all 19 spectra from the first night, the first 20 of the second night, and the last 20 of the second

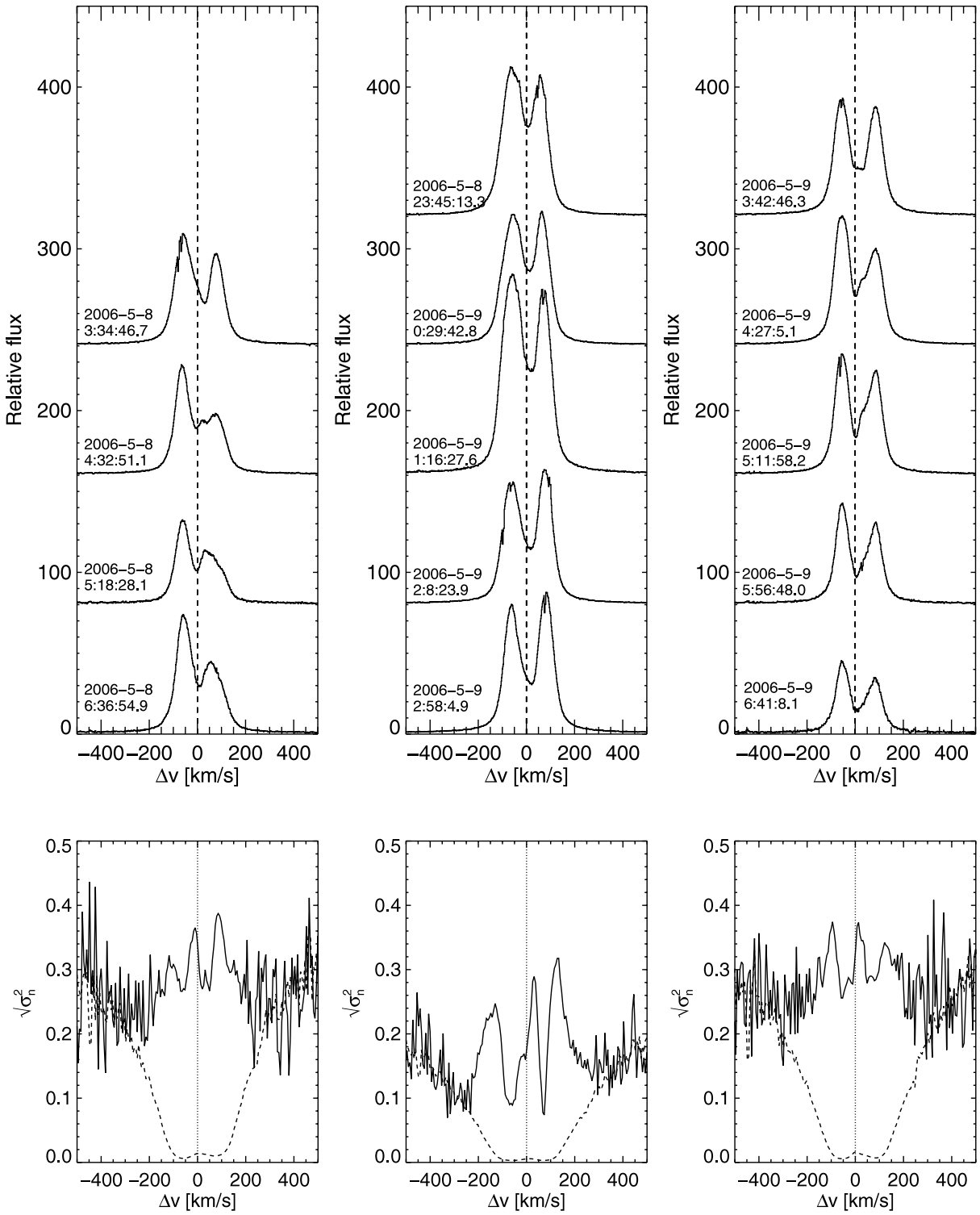

FIG. 2.—*Top*: Normalized average Hα line profiles of 2M 1207 obtained with UVES in 2006 May. *Bottom*: Normalized variance line profiles and zero-variability level.

night, respectively. This way, the individual $(\sigma_n^2)^{1/2}$ values give information about the variations as a function of wavelength on short timescales (within the $\sim$4 hr covered by the 19 or 20 consecutive frames), and a comparison of the different $(\sigma_n^2)^{1/2}$ values can probe changes up to $\sim$1 day.

The normalized variance in the continuum expected from Poisson noise is $\sigma_{n,\mathrm{exp}}^2(\lambda) = \sigma_n^2(\lambda)(\langle\sqrt{I}\rangle/\langle I\rangle)^2$. The zero-variability level $(\sigma_{n,\mathrm{exp}}^2)^{1/2}$ is shown as a dashed line in the bottom panels of Figure 2. Its comparison with the $(\sigma_n^2)^{1/2}$ values shows clear signs of variability in the line profile. Throughout the time series, the variance profile (i.e., the variability as a function of wavelength) features three distinct peaks, roughly at positions of -100 to -150, -20 to $+20$, and $+100$ to $+150$ km s^{-1}. We note that the same structure was seen by Scholz & Jayawardhana (2006) in their Hα time series of 2M 1207. The positions of these peaks (which indicate the velocities of maximum changes in the Hα flux) are roughly coincident with the positions of the two maxima and the minimum in the Hα profile.

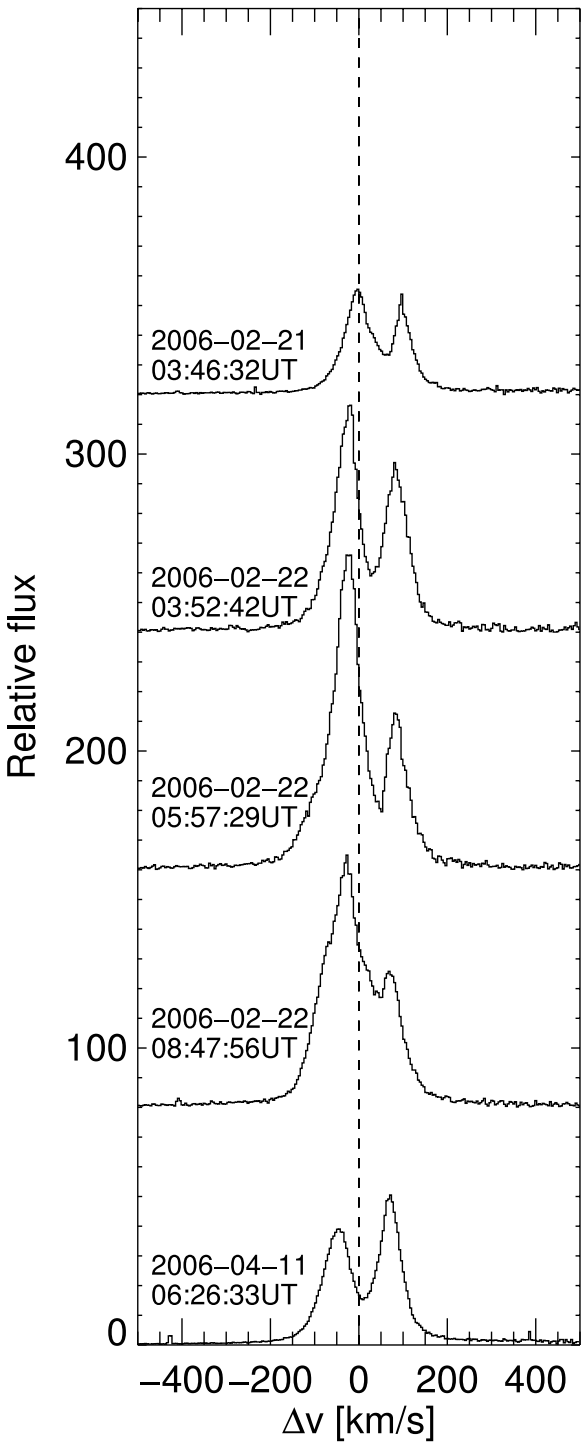

FIG. 3.—Hα line profiles of 2M 1207 obtained with MIKE in 2006 February and April. The data were normalized to the average continuum level near the line.

The variance profile yields only the time average of the changes as a function of wavelength. To study the profile variations in more detail, we examine the change of the flux between consecutive spectra across the line. The relative flux change is given by

$$D_{ji}(\lambda) = \frac{I_{n,j}(\lambda) - I_{n,i}(\lambda)}{2\left[I_{n,j}(\lambda) + I_{n,i}(\lambda)\right]}, \quad (2)$$

where $I_n(\lambda)$ is the normalized profile, i is a running number denoting the exposures, and $j = i + 1$. These relative flux changes $D(\lambda)$ are used to investigate variations as a function of the time lag between two spectra (Johns & Basri 1995). To this end, $D(\lambda)$ is computed not only for two subsequent spectra, but for all pairs of the 59 spectra from 2006 May 8 and 9, i.e., for each time lag $\delta t = t2 - t1 > 0$ sampled by our UVES data. Then, we group the $D(\lambda)$ values in time lag bins of 1 hr (Δt), and calculate the standard deviation $\sigma_{\Delta t}(\lambda)$ of the $D(\lambda)$ values in each of these bins. Finally, we calculate the average of these standard deviations for each time bin over the whole line profile ($\langle \sigma_{\Delta t} \rangle$). The result is shown in Figure 5, where the numbers along the top of the panel indicate the number of data points in each of the time lag bins. The gap is produced by the absence of observations with time lags between $\approx$9 and 16 hr; i.e., the data to the left of this gap correspond to spectra from the same night, and the data to the right correspond to spectra from two different nights. The level of profile variability doubles from $\sim$2% for the shortest time lag (1 hr) to a maximum of $\sim$4% for a time lag of $\sim$8 hr.

To test whether the variations are correlated across the line profile, we computed the correlation coefficient for each pair of spectral bins using the profiles $\langle I_i(\lambda) \rangle$, with $i = 1, \ldots, N$. This results in a correlation matrix $r_{i,j}$ of dimension $N_b \times N_b$, where N_b is the number of spectral bins. The confidence level of each coefficient in the matrix is computed using the error function

$$E_{i,j} = \frac{|r_{i,j}|\sqrt{N_b}}{\sqrt{2}}, \quad (3)$$

such that $1 - E_{i,j}$ is the confidence level necessary for the correlation to be true.

The correlation matrix has been computed for different subgroups of Hα profiles from the UVES run. Figure 6 displays the most interesting correlation matrices $r_{i,j}$ as contour plots. Only values with confidence level >99.9% are considered in this representation. The first two diagrams from the left represent the matrices of each set of 19 consecutive spectra, obtained in the first and the second observing nights, respectively. The cross-shaped pattern seen in the leftmost diagram is peculiar. The center of the cross is offset by $\approx$+25 km s^{-1} to the red side, and it represents the spectral region near the minimum of the line profile (see Fig. 1). Closer examination shows that this pattern stems from a short time interval. This is demonstrated in the rightmost diagram of Figure 6, which displays the correlation matrix for exposures $i = 7, \ldots, 10$, roughly corresponding to the second average profile in the leftmost panel of Figure 2. Clearly, during this time interval, the profile changes near the absorption minimum are uncorrelated with all velocities except for the velocities in close vicinity. The double-square-shaped pattern observed during the second night (Fig. 6, *middle*) is more typical (cf. Johns & Basri 1995). The absence of contours in the upper left and in the lower right of this graph means that red and blue wings vary in an uncorrelated fashion. The range near $v \approx +75$ km s^{-1}, which corresponds to the position of the right emission peak, is particularly well correlated with the whole line.

3.2. *Other Signatures of Accretion*

Our high-S/N UVES spectra allow us to present the first time series for other optical emission lines of 2M 1207. In particular, we detect the Balmer lines up to Hϵ, which is partly blended with Ca II H λ3968.

The shape of the Hβ profile closely follows that of Hα, discussed in detail above. All higher Balmer lines are predominantly characterized by a double-peaked profile, but at times turn into a single-peaked shape. This is demonstrated in Figure 7, which

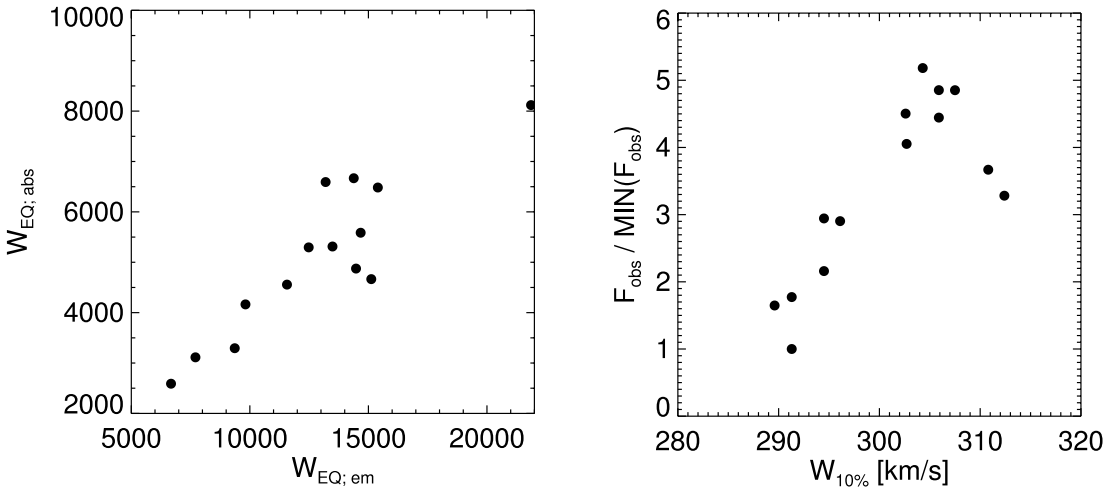

FIG. 4.—Equivalent widths of Gaussian fits to the emission ($W_{eq;em}$) and absorption ($W_{eq;abs}$) components of the Hα line, and normalized total observed flux ($F_{obs} = F_{em} - F_{abs}$) vs. H$\alpha$ 10% width.

shows the contemporaneous Balmer series for two epochs. Each panel in Figure 7 is obtained from an eight-frame average. When present, the absorption minimum is found at roughly the same position for all Balmer lines, but the ratio of the emission fluxes to the left and right of the minimum decreases systematically for the higher Balmer lines; i.e., the lower Balmer lines are red dominated and the higher Balmer lines are blue dominated.

In contrast to the Balmer lines, the Ca II H+K emission is narrow, with a FWHM of only $\sim$20 km s^{-1} (see Table 2). Furthermore, we detect several lines of He I (λ4471, λ5876, λ6678, and λ7066) and the Ca II infrared triplet (hereafter Ca IRT) in emission. All these lines are predominantly detected in accretors, and are therefore thought to be related to the accretion process. The Ca II λ8662 flux was shown to be directly related to the mass accretion rate (Mohanty et al. 2005). The three lines of the Ca IRT appear with roughly similar strength, which is inconsistent with formation in an outflow (Reipurth et al. 1986; Fernández & Comerón 2001). No Na D emission is seen, which is consistent with the prediction of magnetospheric accretion models for low accretion rates (Muzerolle et al. 2001).

We measured W_{eq} and the FWHM of the stronger emission lines discussed above. The continuum was estimated from two 5 Å wide line-free regions to the left and right of the respective line. The observed range of the W_{eq} is reported for each line in Table 2, together with its approximate uncertainty. Given the often loose use of equivalent widths in the literature, it seems appropriate to stress that W_{eq} is associated with considerable errors in objects with faint continuum. This is clear from the numbers given in Table 2. The errors cited in that table do not include systematic uncertainties, which again affect mainly the (faint) continuum, which we discovered in the process of defining the sky extraction area. Since we are interested in relative changes within the UVES data set, systematic uncertainties are not a big concern. However, they should be kept in mind when comparing data obtained with different instruments, and analyzed in different ways by different astronomers.

TABLE 1
SUMMARY OF Hα WIDTH MEASUREMENTS FOR 2M 1207

Date	$W_{10\%}$ (km s^{-1})	References
2002 Apr	$\sim$300[a]	Gizis (2002)
2003 May 8	170–200	Mohanty et al. (2003)
2005 Jan 29–Feb 1	209–215	Scholz et al. (2005a)
2005 Mar 17–19	253–308	Scholz et al. (2005a)
2005 Mar 27–30	279–304	Scholz et al. (2005a)
2006 Feb 21–22	261–281	present work
2006 Apr 11	253	present work
2006 May 8–9	281–322	present work
2006 May 16	320	Whelan et al. (2007)

[a] Low-resolution data; no 10% width measured.

All emission lines are stronger on the second night of the UVES observations, and they are particularly weak toward the end of the first night (around MJD 53,863.25 = UT 05 hr on 2006 May 8). At the same moment, the shape of some of the strongest emission lines underwent a change: (1) He I λ5876 temporarily became flat topped and symmetrical, while it was markedly asymmetric with an extended red wing throughout most of the two nights (see Fig. 8); (2) in Hα, the 10% width was at its minimum, and the deficiency in the red versus the blue peak was particularly strong; (3) in the higher Balmer lines, the red portion of the line disappeared almost completely; and (4) some of the weaker lines nearly disappeared at the same time.

4. DISCUSSION

4.1. *Spectral Variability*

We have examined the optical emission line variability of 2M 1207 at high spectral resolution in data obtained at various epochs through 2006 February, April, and May. In particular, we have presented for the first time a near-continuous spectral sequence from two consecutive nights, with a time resolution of $\approx$12 minutes. The study presented here complements previous work that was characterized by much poorer temporal sampling.

4.1.1. *Short Timescales* (*Days to Hours*)

Scholz et al. (2005a) attributed the drastic changes of the Hα line profile seen in earlier high-resolution spectra of 2M 1207 to a varying viewing angle of the accretion column(s) over the course of the brown dwarf's rotation cycle. The absorption component seemed to appear and reappear on a timescale of $\sim$1 day, an interval approximately coincident with the expected rotation period, and which therefore suggested that the accretion spots moved with respect to the observer. However, with a maximum of three spectra

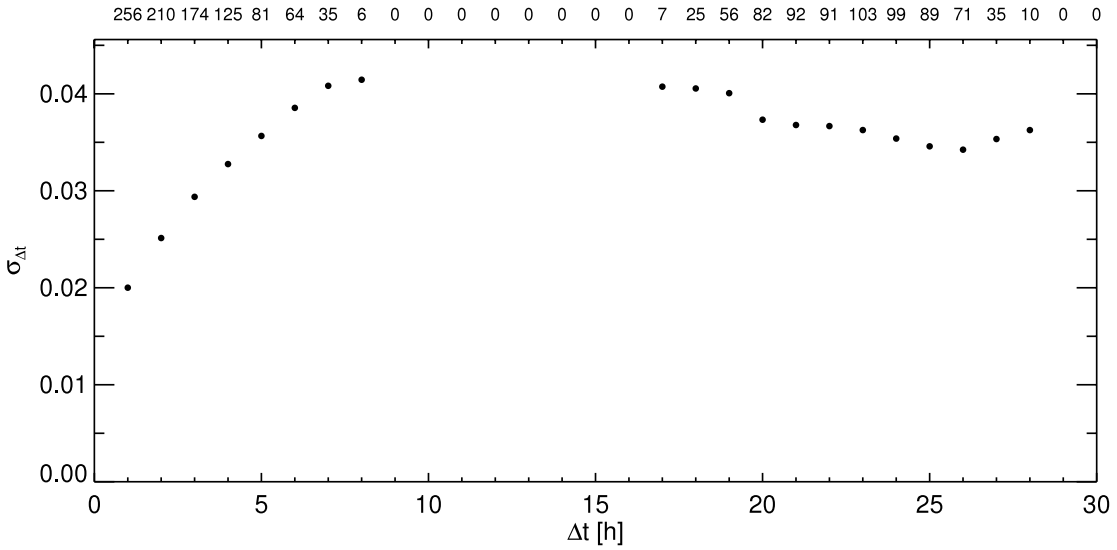

FIG. 5.—Mean of the standard deviation of fractional profile changes $D(\lambda)$ in the Hα line as a function of time lag. The numbers along the top of the panel indicate the number of data points in each of the time lag bins.

per night, the available data did not provide adequate sampling across the presumed rotation cycle.

During the two nights of near-continuous observation in 2006 May there is clear variability present in the Hα emission and other emission lines, albeit much less pronounced and systematic than expected from previous data. Here, we summarize its characteristics. (1) The line profile is double-peaked throughout the two nights, displaying the central absorption reversal characteristic for accretion in star-disk systems seen nearly edge-on. (2) The absorption feature moves between -10 and +40 km s^{-1}. (3) The absorption minimum widens twice during the observations with a time interval of $\sim$23 hr. (4) Variability across the line is inferred from the variance profile and the correlation matrix. (5) The line flux varies by a factor of $\approx$6, correlated with the (small) variations of the 10% width.

The variable redshift and width of the absorption minimum implies that the viewing angle of the absorbing layers of the accretion column changed throughout the observation. Bouvier et al. (2003) explained the radial velocities of the redshifted absorption components of the TTS AA Tau with changes in the structure of the magnetosphere. In this scenario, during times of high observed absorption redshift, an observer at high inclination looks flat onto the magnetic field lines that carry the absorbing material, while low-absorption redshift implies a large angle between the absorbing material and the line of sight. The different viewing angles can be realized by inflating or deflating the star-disk field. In the case of 2M 1207, the observed changes that occur on timescales shorter than the rotation period may suggest that the magnetosphere is somewhat inhomogeneous across stellar longitude. However, the changes are not as dramatic as those seen before. The range of observed redshifts in the absorption minimum of 2M 1207 is comparable to that of AA Tau, but there is no blueshifted absorption. Therefore, outflows do not play a significant role in the formation of the Hα line for 2M 1207.

Although there is no obvious periodicity, the rotation of the star is the most likely cause of the short-term changes in the Hα profile summarized above. We have shown that the fractional profile changes reach a maximum after a time lag of $\sim$8 hr, and that they remain high on a plateau for larger time lags. (The exact position of the maximum is unclear due to the absence of data with time lags between 9 and 15 hr.) This timescale is roughly consistent with one-half the expected rotation period, and therefore with the time interval in which maximum changes due to rotational effects are expected.

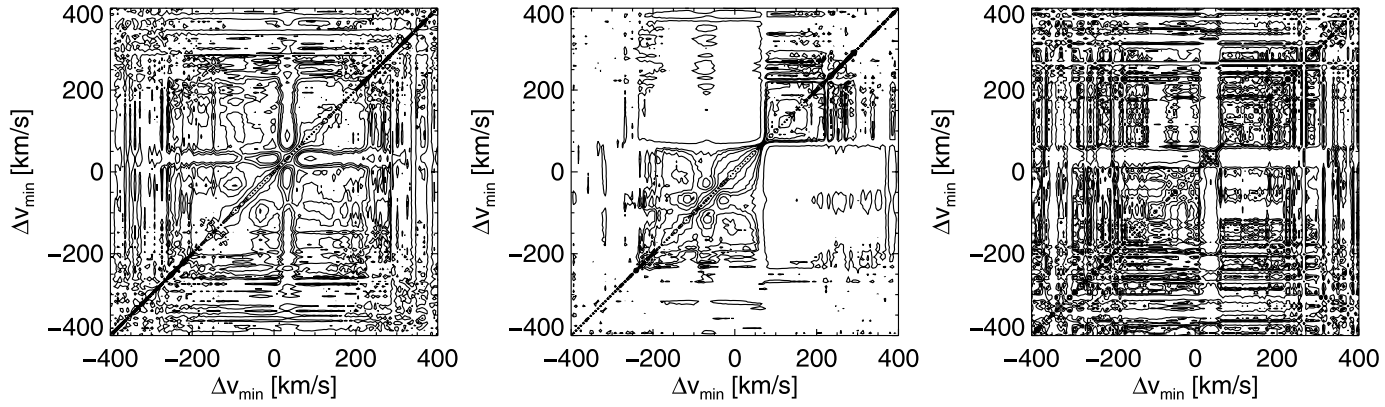

FIG. 6.—Correlation matrix of Hα for different subsets of exposures (denoted i) obtained on 2006 May 8 and 9. *Left*: $i = 1, \ldots, 19$. *Middle*: $i = 20, \ldots, 38$. *Right*: $i = 7, \ldots, 10$.

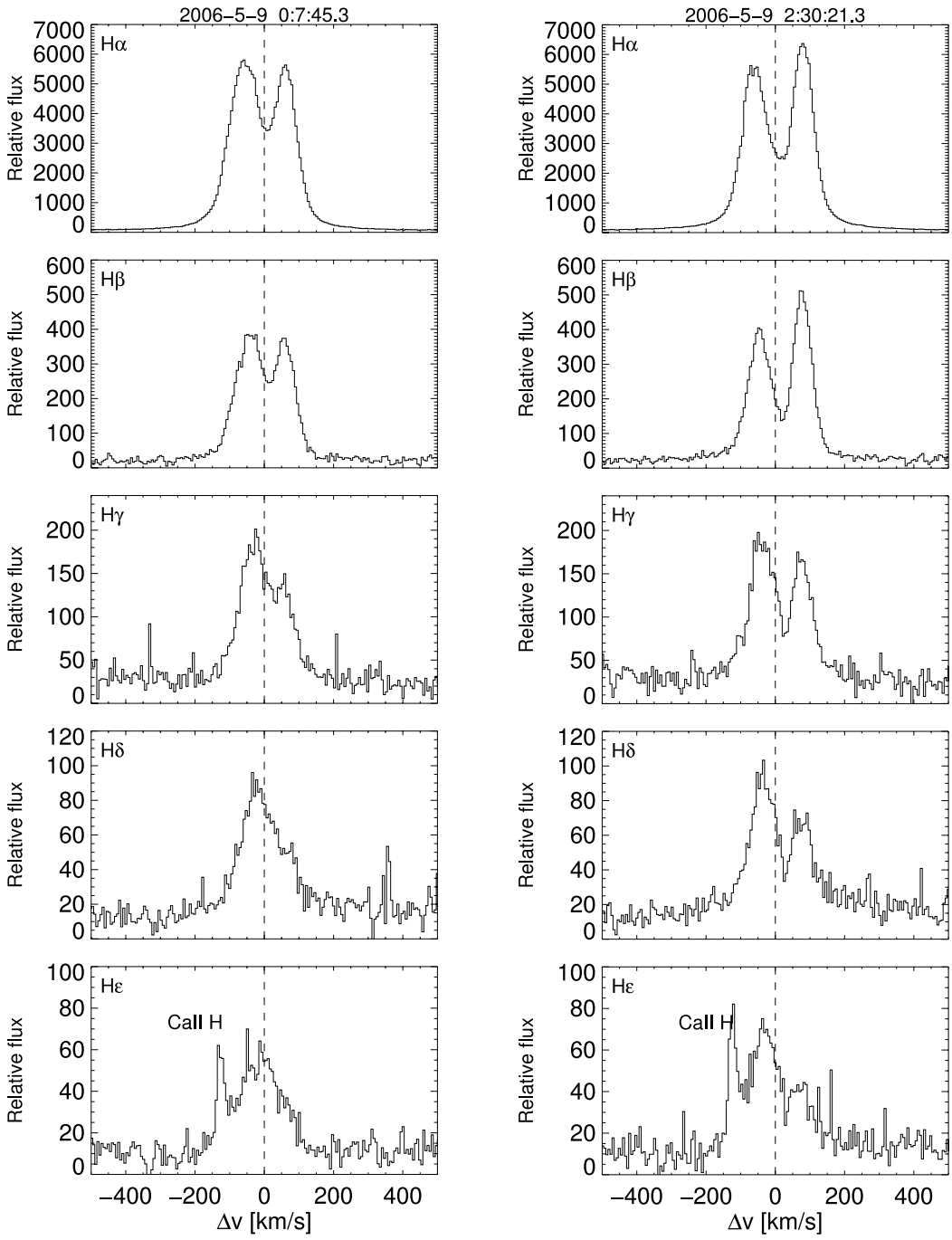

FIG. 7.—Contemporaneous Balmer emission line profiles (Hα to Hϵ) for two epochs during the UVES run (eight-frame averages).

If possible contributions from chromospheric activity and winds are neglected, the emission line flux is expected to be a measure for the accretion rate, and this is supported by its correlation with the 10% width. This correlation is not trivial, because the fit function's normalization is independent of its width, unlike in a canonical Gaussian. We conclude from the correlation observed between the equivalent widths of the emission and the absorption components (Fig. 4) that the amount of absorbing material is proportional to the total amount of material crossing the line of sight.

With the exception of the Ca II H+K lines, the strong emission lines (higher Balmer lines, He I, and Ca IRT) follow the Hα emission closely in their shape and variability, which indicates a common origin, i.e., accretion, and that chromospheric contributions are not significant. In particular, the lines of the Balmer series are mostly double peaked throughout our observations. Only the higher lines Hδ and Hϵ turn at times into a single-peaked shape.

4.1.2. *Intermediate Timescales* (*Weeks to Months*)

The Hα line is characterized by a double-peaked profile in all spectra obtained from 2006 February to May. In the spectra from February and April, the redshift of the absorption feature is systematically larger with respect to the observations from May, and consequently, the line profiles observed in February and April are also more asymmetric than the ones from May. However, in the data from 2006, the variations are smoother and less dramatic than those from 2005, for which Scholz et al. (2005a) reported alternating single- and double-peaked profiles within individual observing nights.

TABLE 2
Equivalent Widths and FWHM for Detected Emission Lines

Identification	W_{eq}[a] (Å)	Typical Error[a, b] (Å)	FWHM[c] (km s^{-1})
Hβ	4.5–47.1	~6	180
Hγ	0.3–13.5	~2	180
Hδ	...	...	168
Hϵ+Ca II H	...	...	144
Ca II K	...	...	18
He I λ5876	1.8–9.1	~2	30
Hα	145–394	~45	210
He I λ6678	0.9–2.4	~2	18
Ca II λ8498	0–0.6	~0.35	12
Ca II λ8542	0–0.3	~0.25	12
Ca II λ8662	0–0.4	~0.3	12

[a] No equivalent widths are given for the higher Balmer lines and for Ca II H+K because of the low continuum.
[b] Errors for the equivalent width are estimated by assuming a 15% uncertainty in the continuum flux.
[c] Measured in an average spectrum that represents the typical line profile for 2M 1207 during the observation.

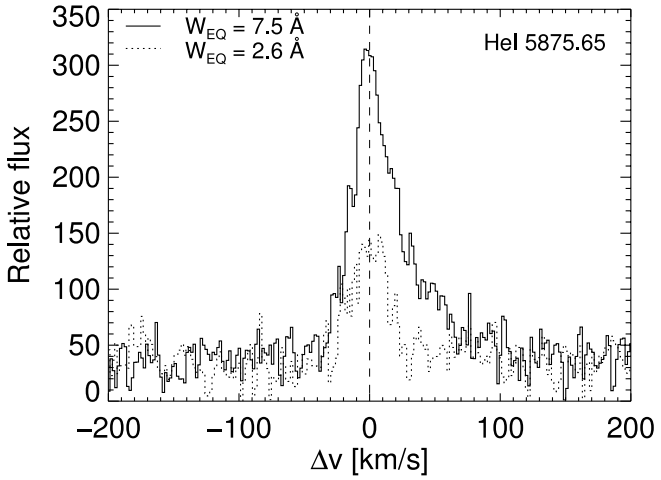

Fig. 8.—Two spectra in the region of He I λ5876 showing the change from the typical profile with extended red wing (*solid line*) to the weak, symmetric line (*dotted line*).

If the previous assumption of a high-inclination system rotating at a rate of ~1 day is correct, the data from 2006 are compatible with a rather homogeneous distribution of accretion elements, i.e., magnetosphere, across the (sub)stellar longitudes, with smaller inhomogeneities as discussed in § 4.1.1. In contrast, during 2005, the absorption reversal appeared and disappeared within one rotation cycle, which implies strong variations in the accretion structure across the stellar surface. We conclude that the distribution of the accretion elements or the structure of the magnetosphere changed within ~1 yr. In both years, 2005 and 2006, the mass accretion rate, as inferred from the 10% width of the Hα emission (see, e.g., Natta et al. 2004, and § 4.2), showed fluctuations by a factor of ~2 on timescales of weeks to months (cf. Table 1).

4.1.3. *Long Timescales* (*Years*)

Three years have passed since the first high-resolution spectrum of 2M 1207 was obtained, and in this period there seems to be a tendency toward an enhanced mass accretion rate. Note, however, that the large Hα equivalent width measured by Gizis (2002) in a low-resolution spectrum counteracts this trend, and fluctuations on shorter timescales (discussed above) may be superposed on the long-term evolution. Further observations are required to confirm our speculation about the secular evolution of the Hα emission.

4.2. *Accretion Rate and Magnetic Field*

Natta et al. (2004) have parameterized the accretion rate as a function of $W_{10\%}$ for TTSs and brown dwarfs. From their equation (1), we find an accretion rate of $10^{-10.1}$–$10^{-9.8}\,M_\odot\,\mathrm{yr}^{-1}$ for the range of Hα 10% widths measured for 2M 1207 during the UVES run in 2006 May. In previous measurements, $\dot{M}_{\rm acc}$ was as low as $\sim 10^{-11.2}\,M_\odot\,\mathrm{yr}^{-1}$; i.e., 2M 1207 changes its accretion rate by a factor of 2 on the timescale of days, and by at least 1 order of magnitude on a timescale of years.

In Figure 9, we put 2M 1207 in context with other accreting (sub)stellar objects. A correlation between accretion rate and mass ($\dot{M}_{\rm acc} \sim M^{\alpha}$ with $\alpha \approx 2$) has been reported in the literature. In Figure 9, we display this relation using data from the references given in Muzerolle et al. (2005). The range of $\dot{M}_{\rm acc}$ inferred from all available data of 2M 1207 is indicated by large circles connected by a vertical line.

Various explanations have been proposed for the correlation between $\dot{M}_{\rm acc}$ and M, and its large (>2 dex) scatter. Padoan et al. (2005) see in the $\dot{M}_{\rm acc}$-M relation a consequence of large-scale Bondi-Hoyle accretion. In their scenario, the scatter is produced by the different physical conditions in different star-forming environments. Alexander & Armitage (2006) assume that the $\dot{M}_{\rm acc}$-M relation reflects the initial parameters of the disk-star system, and show that the scatter can be reproduced by a combination of varying disk initial parameters and the viscous evolution of the disk, in the course of which the mass accretion rate decreases. According to Gregory et al. (2006) the $\dot{M}_{\rm acc}$-M relation arises naturally from models of magnetospheric accretion if one assumes a realistic field geometry. Finally, Mohanty et al. (2005) suggest that declining disk ionization with decreasing stellar mass is the origin of the $\dot{M}_{\rm acc}$-M relation, implying that most of the scatter is due to intrinsic variability in accretion rates. This view is disputed by Natta et al. (2006), who do not find that strong variations of the near-IR emission lines are indicative of accretion in a sample of 14 objects from the ρ Oph star-forming region. On the other hand, it has been demonstrated for a few examples of individual objects that accretion rates do indeed vary substantially (Gullbring et al. 1996; Alencar et al. 2005; Scholz et al. 2005a; Scholz & Jayawardhana 2006). We point out that the range of mass accretion rates derived for 2M 1207 is comparable to the spread in the $\dot{M}_{\rm acc}$-M relation. Therefore, variability might indeed explain this spread. Repeated measurements of $\dot{M}_{\rm acc}$ for known accretors will help to verify our suggestion.

An alternative method for deriving accretion rates has been proposed by Mohanty et al. (2005). They established that both classical TTSs and brown dwarfs follow a linear correlation between the Ca II λ8662 emission flux and $\dot{M}_{\rm acc}$ that is determined independently from Hα modeling or veiling measurements. Following their recipe, we estimate the continuum flux $F_{\rm cont}$ of 2M 1207 at 8662 Å from the synthetic DUSTY spectra of Allard et al. (2000). We adopt $T_{\rm eff} = 2800$ K, $\log g = 4.0$, and negligible veiling (see discussion in Mohanty et al. 2005 for justification of these choices). The line flux is then given by $F_{\rm Ca\,II} = F_{\rm cont} W_{\rm eq}$. For the highest equivalent width measured in 2006 May, this results in $\log F_{\rm Ca\,II}[\mathrm{erg\ cm^{-2}\ s^{-1}}] \approx 5.1$, and the fit relation for the

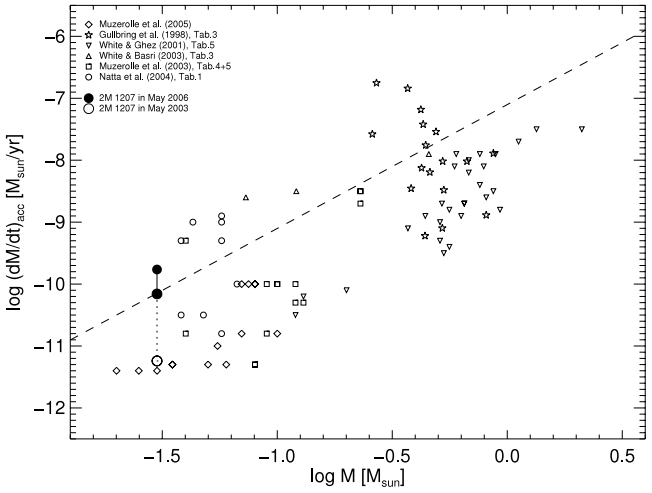

FIG. 9.—Relation between mass and mass accretion rate for substellar objects. Data is from the literature cited by Muzerolle et al. (2005).

low-mass sample of Mohanty et al. (2005) yields an accretion rate of $\dot{M}_{\rm acc} \approx 10^{-10.3}\ M_\odot\ {\rm yr}^{-1}$. This is in rough agreement with the value we derived above from the Hα 10% width. We caution that using the Ca II λ8662 line for estimating the mass accretion rate assumes a negligible contribution from activity. This seems to be true for brown dwarfs on a statistical basis ("the λ8662 component occurs almost exclusively in accreting objects"; Mohanty et al. 2005), and for 2M 1207 in particular, by the lack of measurable effects from chromospheric emission in other lines.

According to Koenigl (1991) the mass accretion rate of TTSs is related to their magnetic field strength, $B \sim \dot{M}^{1/2} M_*^{1/4} R_*^{-3} R_t^{7/4}$. We assume $R_t \sim 2R_*$ for the disk truncation radius (Muzerolle et al. 2000). The mass and radius of 2M 1207 are $M_* = 0.03\ M_\odot$ and $R_* = 0.27\ R_\odot$ (Chabrier et al. 2000). Taking account of the scaling factors, the average accretion rate of 2M 1207 observed in 2006 May ($\dot{M} \sim 10^{-10}\ M_\odot\ {\rm yr}^{-1}$) yields an approximate value for the surface field of $B \approx 200$ G. For a TTS with $0.8\ M_\odot$, $1.5\ R_\odot$, and $\dot{M} \sim 10^{-8}\ M_\odot$, the same equation yields a surface field of $\approx$600 G. This validates the remark made by Scholz & Jayawardhana (2006), who, without citing numbers for the field strength, argued that the magnetic field for a typical brown dwarf is expected to be roughly half that of a typical TTS.

The magnetic field of TTSs obtained this way is somewhat lower than measured values, which are typically in the kilogauss range (e.g., Yang et al. 2005, and references therein). There are, however, considerable uncertainties connected with the use of the Koenigl relation, such as the simplified assumption of a dipolar field and the location of the inner disk radius with respect to the corotation radius that determines the scaling factor. Given these ambiguities, the order of magnitude agreement between the estimated and observed fields is plausible.

4.3. *Accretion Versus Activity in TWA Brown Dwarfs*

Given the presence of a magnetic field, inferred from the accretion rate, the absence of strong magnetic activity on 2M 1207 is remarkable. A very stringent upper limit to its X-ray emission was placed by a 50 ks *Chandra* observation (Gizis & Bharat 2004). The radio emission was constrained to the lowest value among the brown dwarfs in the TWA (Osten & Jayawardhana 2006). In Table 3, we summarize the accretion and activity measures for all four TWA brown dwarfs.

The data in Table 3 have been collected from the literature, except for the X-ray data for SSSPM 1102. This object was identified as a probable substellar TWA member in a recent proper motion study of the Supercosmos Sky Survey data (Scholz et al. 2005b). SSSPM 1102 is in the field of view of an archived *XMM-Newton* observation (ObsID 0112880201). We ran the standard Science Analysis System source detection process, and found no X-ray source at the optical position of SSSPM 1102. To estimate an upper limit to its X-ray luminosity, we measured the counts at the expected position of SSSPM 1102 and in an annulus around this position (representing the background). After applying the appropriate area scaling factor and extracting the on-source time from the exposure map, an upper limit to the net source count rate was estimated using the algorithm of Kraft et al. (1991). The distance to SSSPM 1102 has been given by Mamajek (2005) ($d \sim 43$ pc). This yields $L_{\rm X} < 5.3 \times 10^{26}$ erg s^{-1} in the 0.5–10 keV band.

It is constructive to compare 2M 1207 to TWA 5 B, the best-studied substellar object in the TWA after 2M 1207. Matching their properties shows the dichotomy of one brown dwarf that accretes but is not magnetically active, and another brown dwarf that is magnetically active but does not accrete. Presumably, some mechanism suppresses activity in accreting substellar objects, as seems to be the case for classical TTSs (Preibisch et al. 2005; Telleschi et al. 2007). Possible explanations that have been put forth in the context of classical TTSs are changes in the magnetic field structure and/or heating process of the corona as a result of accretion. The absence of magnetic activity on 2M 1207 is further surprising, as accreting substellar objects with similar magnetic field strength, e.g., V410 Anon 13, have been shown to be X-ray emitters (Muzerolle et al. 2000; Güdel et al. 2007). For the substellar regime, the relation between accretion and X-ray luminosity has not yet been established on a statistical sample. If such a relation, as suggested by 2M 1207 and TWA 5 B, is confirmed, it would provide one more piece of evidence for the TTS-like character of brown dwarfs. X-ray and radio studies of the remaining two TWA brown dwarfs, both of which are nonaccreting, should be useful.

TABLE 3
ACTIVITY AND ACCRETION MEASURES OF ALL KNOWN BROWN DWARFS IN TWA

Designation	IR Excess	$W_{\rm H\alpha;10\%}$ (km s^{-1})	$L_{\rm X}$ (erg s^{-1})	$L_{\rm R}$ (10^{14} erg s^{-1} Hz^{-1})	FUV	References
TWA 5B	...	162	4×10^{27}	<2.0	...	..., 1, 2, 3, ...
2M 1207	Y	170–320	$<1.2 \times 10^{26}$	<0.98	Y	4, 5, 6, 3, 7
2M 1139	N	111	...	<0.5	...	4, 1, ..., 8, ...
SSSPM 1102	...	194	$<5.3 \times 10^{26}$	<1.6	...	..., 1, 9, 3, ...

REFERENCES.—(1) Mohanty et al. 2003; (2) Tsuboi et al. 2003; (3) Osten & Jayawardhana 2006; (4) Riaz et al. 2006; (5) See references in this paper; (6) Gizis & Bharat 2004; (7) Gizis et al. 2005; (8) Burgasser & Putman 2005; (9) This paper.

5. CONCLUSIONS

A substantial number of high-resolution spectroscopic observations have been collected for the brown dwarf 2M 1207. These data have allowed us to study its accretion variability on timescales from hours to ~3 yr. While small variations are obviously present throughout the rotation (~1 day), major changes in the structure of accretion may take place over months or years. A summary of all Hα width measurements suggests a trend toward increasing accretion rate during the last 3 years. However, it is not clear if this trend reflects erratic changes or a systematic evolution. All in all, our dedicated monitoring has shown that the accretion pattern on 2M 1207 is probably more complex than expected. It comprises long-term changes of the accretion rate and (maybe independently) of the flow structure (months to years), variations on the timescale of the rotation rate (hours to days), and possibly on even shorter timescales, as suggested by our high temporal resolution data.

2M 1107 is among the lowest mass dwarfs with a measured mass accretion rate. The values derived from the various observations obtained in a time span of ~3 yr differ by nearly 2 dex, similar to (and possibly explaining) the scatter observed in the relation between accretion rate and stellar mass. Whether accretion variability is decisive for shaping the $\dot{M}_{\rm acc}$-M relation will be established in future systematic spectroscopic studies across a wide mass range.

This paper is based on data collected under the ESO program 077.C-0323. B. S. acknowledges financial support from ASI contract ASI-INAF I/023/05/0. B. S. wishes to thank S. Randich and S. Mohanty for useful discussions on the UVES pipeline analysis and brown dwarf emission line spectra. R. J. and A. S. acknowledge support from an NSERC grant to R. J.

Facilities: VLT:Kueyen (UVES)

REFERENCES

Alencar, S. H. P., Basri, G., Hartmann, L., & Calvet, N. 2005, A&A, 440, 595
Alexander, R. D., & Armitage, P. J. 2006, ApJ, 639, L83
Allard, F., Hauschildt, P. H., & Schweitzer, A. 2000, ApJ, 539, 366
Allers, K. N., Kessler-Silacci, J. E., Cieza, L. A., & Jaffe, D. T. 2006, ApJ, 644, 364
Ballester, R., Modigliani, A., Boitquin, O., Cristiani, S., Hanuschik, R., Kaufer, A., & Wolf, S. 2000, Messenger, 101, 31
Barrado y Navascués, D., Mohanty, S., & Jayawardhana, R. 2004, ApJ, 604, 284
Bouvier, J., et al. 2003, A&A, 409, 169
Burgasser, A. J., & Putman, M. E. 2005, ApJ, 626, 486
Chabrier, G., Baraffe, I., Allard, F., & Hauschildt, P. 2000, ApJ, 542, 464
Chauvin, G., Lagrange, A.-M., Dumas, C., Zuckerman, B., Mouillet, D., Song, I., Beuzit, J.-L., & Lowrance, P. 2004, A&A, 425, L29
———. 2005, A&A, 438, L25
Edwards, S., Cabrit, S., Strom, S. E., Heyer, I., Strom, K. M., & Anderson, E. 1987, ApJ, 321, 473
Fernández, M., & Comerón, F. 2001, A&A, 380, 264
Gizis, J. E. 2002, ApJ, 575, 484
Gizis, J. E., & Bharat, R. 2004, ApJ, 608, L113
Gizis, J. E., Shipman, H. L., & Harvin, J. A. 2005, ApJ, 630, L89
Gregory, S. G., Jardine, M., Simpson, I., & Donati, J.-F. 2006, MNRAS, 371, 999
Güdel, M., et al. 2007, A&A, 468, 353
Gullbring, E., Petrov, P. P., Ilyin, I., Tuominen, I., Gahm, G. F., & Loden, K. 1996, A&A, 314, 835
Hamann, F. 1994, ApJS, 93, 485
Hartigan, P., Edwards, S., & Ghandour, L. 1995, ApJ, 452, 736
Hartmann, L., Hewett, R., & Calvet, N. 1994, ApJ, 426, 669
Jayawardhana, R., Ardila, D. R., Stelzer, B., & Haisch, K. E., Jr. 2003a, AJ, 126, 1515
Jayawardhana, R., Mohanty, S., & Basri, G. 2003b, ApJ, 592, 282
Johns, C. M., & Basri, G. 1995, AJ, 109, 2800
Koenigl, A. 1991, ApJ, 370, L39
Kraft, R. P., Burrows, D. N., & Nousek, J. A. 1991, ApJ, 374, 344
Luhman, K. L., et al. 2005, ApJ, 631, L69
Mamajek, E. E. 2005, ApJ, 634, 1385
Martín, E. L. 1998, AJ, 115, 351
Mohanty, S., Jayawardhana, R., & Barrado y Navascués, D. 2003, ApJ, 593, L109
Mohanty, S., Jayawardhana, R., & Basri, G. 2005, ApJ, 626, 498
Mundt, R. 1984, ApJ, 280, 749
Muzerolle, J., Briceño, C., Calvet, N., Hartmann, L., Hillenbrand, L., & Gullbring, E. 2000, ApJ, 545, L141
Muzerolle, J., Calvet, N., & Hartmann, L. 2001, ApJ, 550, 944
Muzerolle, J., Luhman, K. L., Briceño, C., Hartmann, L., & Calvet, N. 2005, ApJ, 625, 906
Natta, A., Testi, L., Comerón, F., Oliva, E., D'Antona, F., Baffa, C., Comoretto, G., & Gennari, S. 2002, A&A, 393, 597
Natta, A., Testi, L., Muzerolle, J., Randich, S., Comerón, F., & Persi, P. 2004, A&A, 424, 603
Natta, A., Testi, L., & Randich, S. 2006, A&A, 452, 245
Osten, R. A., & Jayawardhana, R. 2006, ApJ, 644, L67
Padoan, P., Kritsuk, A., Norman, M. L., & Nordlund, Å. 2005, ApJ, 622, L61
Preibisch, T., et al. 2005, ApJS, 160, 401
Reipurth, B., Bally, J., Graham, J. A., Lane, A. P., & Zealey, W. J. 1986, A&A, 164, 51
Riaz, B., Mullan, D. J., & Gizis, J. E. 2006, ApJ, 650, 1133
Scholz, A., & Jayawardhana, R. 2006, ApJ, 638, 1056
Scholz, A., Jayawardhana, R., & Brandeker, A. 2005a, ApJ, 629, L41
Scholz, R.-D., McCaughrean, M. J., Zinnecker, H., & Lodieu, N. 2005b, A&A, 430, L49
Sterzik, M. F., Pascucci, I., Apai, D., van der Bliek, N., & Dullemond, C. P. 2004, A&A, 427, 245
Telleschi, A., Güdel, M., Briggs, K. R., Audard, M., & Palla, F. 2007, A&A, 468, 425
Tsuboi, Y., Maeda, Y., Feigelson, E. D., Garmire, G. P., Chartas, G., Mori, K., & Pravdo, S. H. 2003, ApJ, 587, L51
Whelan, E. T., Ray, T. P., Randich, S., Bacciotti, F., Jayawardhana, R., Testi, L., Natta, A., & Mohanty, S. 2007, ApJ, 659, L45
White, R. J., & Basri, G. 2003, ApJ, 582, 1109
Yang, H., Johns-Krull, C. M., & Valenti, J. A. 2005, ApJ, 635, 466